Frontiers of Information Technology & Electronic Engineering
www.jzus.zju.edu.cn; engineering.cae.cn; www.springerlink.com
ISSN 2095-9184 (print); ISSN 2095-9230 (online)
E-mail: jzus@zju.edu.cn

A mechanical reliability study of 3-dB waveguide hybrid couplers in submillimeter and terahertz bands*

Zhongqian NIU[1], Bo ZHANG[†‡1], Daotong LI[2], Dongfeng JI[1], Yang LIU[1], Yinian FENG[1], Tianchi ZHOU[1], Yaohui ZHANG[1], Yong FAN[1]

[1]*School of Electronic Science and Engineering, University of Electronic Science and Technology of China, Chengdu 611731, China*

[2]*Center of Aerocraft TT&C and Communication, Chongqing University, Chongqing 400044, China*

[†]E-mail: zhangbouestc@yeah.net

Received May 12, 2020; Revision accepted Sept. 23, 2020; Crosschecked July 19, 2021

Abstract: This paper presents a mechanical reliability study of 3-dB waveguide hybrid couplers in submillimeter and terahertz bands. To show the necessity of improving the mechanical properties of the coupler's branch in submillimeter and terahertz bands, a comprehensive study regarding the displacement of hybrid branch variation with varying width-length ratio and height-length ratio has been completed. In addition, a modified 3-dB waveguide hybrid coupler is designed and presented. Compared with the traditional branch structure, the proposed hybrid consists of a modified middle branch with circular cutouts at the top and bottom on both sides instead of the traditional rectangle branch, which increases the branch size and improves its mechanical reliability while achieving the same performance. Simulation results show that the deformation of the modified hybrid branch is 22% less than those of other traditional structure designs under the same stress. In practice, a vibration experiment is set up to verify the mechanical reliability of hybrid couplers. Measurement results show that the experiment deteriorates the coupling performance. Experimental results verify that the performance of the novel structure coupler is better than that of a traditional structure branch hybrid coupler under the same electrical properties.

Key words: Directional coupler; 3-dB waveguide hybrid coupler; Submillimeter-wave device; Terahertz circuit; Mechanical reliability

https://doi.org/10.1631/FITEE.2000229 **CLC number:** TN61

1 Introduction

The terahertz (THz) region, which includes the millimeter and submillimeter wave ranges, is situated between the microwave and infrared frequencies. Given its special position in the electromagnetic spectrum, submillimeter and THz technology shows significant research prospects in fields such as astrophysics, wireless communication, and passive detection (Graham-Rowe, 2007; Hosako et al., 2007; Tonouchi, 2007; Armstrong, 2012).

Directional couplers have been studied since the 1940s, and have resulted in various design techniques for both waveguide and substrate-based components. They are widely used in submillimeter and THz systems such as radar receivers (Chattopadhyay, 2011; Kooi et al., 2012; Dhillon et al., 2017), power amplifiers (Malo-Gomez et al., 2009; Siles et al., 2011), and high-speed communication systems (Chen et al., 2016a, 2016b). In these systems, couplers play an important role in functions regarding power distribution/synthesis or phase change. Therefore, a study of directional couplers in the THz band possesses a very high application value.

‡ Corresponding author

* Project supported by the National Natural Science Foundation of China (Nos. 61771116 and 62022022), the National Key R&D Program of China (No. 2018YFB1801502), and the China Postdoctoral Science Foundation (No. 2021TQ0057)

ORCID: Zhongqian NIU, https://orcid.org/0000-0001-8852-3516; Bo ZHANG, https://orcid.org/0000-0002-8119-5000; Daotong LI, https://orcid.org/0000-0003-4413-4847

There are many design structures of substrate-based hybrids with diverse fabrication complexity that offer improved hybrid performance in the microwave band (Phromloungsri et al., 2006; Müller et al., 2011). However, the size of the circuit decreases sharply in the THz band, which leads to difficulties in processing a traditional microstrip line coupler. The branch waveguide 90° hybrid coupler shows great advantages for high-frequency (submillimeter wave to THz wave) applications because of its simple structure, high isolation, small insertion loss, and high power capacity. Even if the structure of the branch waveguide is simple, the machining requirement for the THz circuit is still a significant challenge. The branches of a hybrid are very tiny at such a high frequency and are very sensitive to the size. To guarantee the great performance, some work has been done using high-precision micromachining technology (Sobis et al., 2008; Rashid et al., 2014, 2016; Gonzalez et al., 2017; Hesper et al., 2017). Others use another processing technology, i.e., micro-electro-mechanical system (MEMS) technology (Lubecke et al., 1998; Zhou et al., 2014), which is very expensive and time-consuming.

When used for an aerospace application or in other extreme environmental applications, high performance is not the only advantage that needs to be considered. For example, good mechanical reliability and reasonable cost are also very important. A comprehensive study regarding the displacement of hybrid branch variation with a different width-length ratio and height-length ratio has been completed, showing the necessity of improving the mechanical properties of the coupler's branch. Moreover, a modified 90° waveguide hybrid coupler structure (Niu et al., 2019a) with circular cutouts at the top and bottom on both sides of the main branch is compared with the traditional rectangle branch structure in the mechanical property study. Mechanical simulation results show that deformation of the modified coupler structure branch is 22% less than those of other traditional structure designs under the same stress, which was also verified in a vibration experiment when the limitation in machining technology was relaxed and the mechanical reliability was improved. Submillimeter and THz circuits have already penetrated into aerospace applications, but an analysis of circuit reliability was rarely reported. This study will be helpful for the space application of submillimeter and THz circuits and provides a theoretical basis for the assembly processing and risk control of hybrid coupler circuits.

2 Theory and design of the hybrid coupler

The design of a traditional waveguide hybrid coupler is often based on several rectangle shunt-branch structures (Fig. 1).

A waveguide is often fabricated on a metal block. After processing, some metal branches remain. The waveguide hybrid design in Reed (1958) exhibits the optimal performance for multi-branch structures. Hence, for wider operation bandwidth and better performance, multi-branch waveguide couplers (more than five shunt branches) have been designed (Lubecke et al., 1998; Sobis et al., 2008; Rashid et al., 2014, 2016; Zhou et al., 2014; Gonzalez et al., 2017; Hesper et al., 2017). However, based on Niu et al. (2019a), if the coupling rate and the center frequency are determined, then the more shunt branches the coupler has, the smaller each size of the shunt branch. As a result, the metal branch becomes narrower in these studies. The metal branches of the hybrid are very tiny and any compressive stress can cause bending or even breaking of the metal branches, which will influence the hybrid ratio and phase imbalance and significantly deteriorate the performance.

To widen the metal branch for better mechanical properties, an improved three-branch hybrid coupler was presented in Niu et al. (2019b). The design procedure is based on the odd and even mode analysis method and ABCD matrix. The initial theory is based on the structure in Fig. 2. The signal is fed from port 1 (P1), and port 2 (P2) is the throughout port. Port 3 (P3) is the coupling port, where the coupling ratio can be

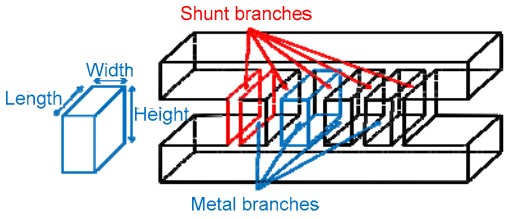

Fig. 1 Schematic of a traditional five-branch waveguide hybrid coupler

manually designed. Port 4 (P4) is the isolation port. In addition, the phase difference between P2 and P3 is 90°.

Then, according to the odd and even mode analysis method, each part of the waveguide branch can be regarded as a two-port network. For the analysis of cascaded two-port networks, the ABCD matrix can be used to implement the analysis. The improved hybrid design structure is divided into several sub-networks, and each represents a branch or main waveguide section. The ABCD matrix can then be expressed as the multiplication of these networks' matrices:

$$\begin{cases} \begin{bmatrix} A & B \\ C & D \end{bmatrix}_{\mathrm{e}} = \begin{bmatrix} 1 & \mathrm{j}W_1 \tan\left(\dfrac{\theta_{T_1}}{2}\right) \\ 0 & 1 \end{bmatrix} \begin{bmatrix} 0 & \mathrm{j}\tan\theta_{W_2} \\ \mathrm{j}\tan\theta_{W_2} & 0 \end{bmatrix} \\ \quad \cdot \begin{bmatrix} 0 & \mathrm{j}k\tan\theta_{W_3} \\ \mathrm{j}k\tan\theta_{W_3} & 0 \end{bmatrix} \begin{bmatrix} 1 & \mathrm{j}W_1 \tan\left(\dfrac{\theta_{T_2}}{2}\right) \\ 0 & 1 \end{bmatrix} \\ \quad \cdot \begin{bmatrix} 0 & \mathrm{j}k\tan\theta_{W_3} \\ \mathrm{j}k\tan\theta_{W_3} & 0 \end{bmatrix} \begin{bmatrix} 0 & \mathrm{j}\tan\theta_{W_2} \\ \mathrm{j}\tan\theta_{W_2} & 0 \end{bmatrix} \\ \quad \cdot \begin{bmatrix} 1 & \mathrm{j}W_1 \tan\left(\dfrac{\theta_{T_1}}{2}\right) \\ 0 & 1 \end{bmatrix}, \\ \begin{bmatrix} A & B \\ C & D \end{bmatrix}_{\mathrm{o}} = \begin{bmatrix} A_{\mathrm{e}}\left(-\dfrac{1}{p}\right) & B_{\mathrm{e}}\left(-\dfrac{1}{p}\right) \\ C_{\mathrm{e}}\left(-\dfrac{1}{p}\right) & D_{\mathrm{e}}\left(-\dfrac{1}{p}\right) \end{bmatrix}, \end{cases} \tag{1}$$

where $k=l_2/l_1$, θ is the electrical length in the waveguide, $\theta_l = \pi l\sqrt{(2/\lambda_0)^2-(1/a)^2}$ ($l\in\{T_1, T_2, W_2, W_3\}$, and these parameters are illustrated in Fig. 2), a is the main waveguide width, λ_0 is the free-space wavelength, $p=\tan(\theta_l/2)$, and the subscripts "e" and "o" represent the even and odd modes, respectively.

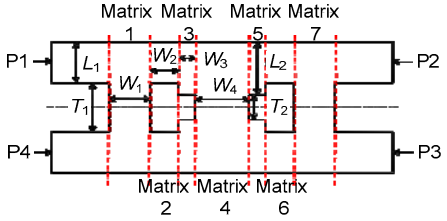

Fig. 2 Initial structure of the improved three-branch hybrid coupler

Then, the transmission terms can be expressed by ABCD matrices as

$$\begin{cases} \dfrac{1}{2}T_i = \dfrac{1}{A+B+C+D}, \\ \dfrac{1}{2}\Gamma_i = \dfrac{A+B-C-D}{2(A+B+C+D)}, \end{cases} \tag{2}$$

where T is the transmission coefficient, Γ is the reflection coefficient, and the index i is either "e" or "o."

Based on the odd and even mode analysis method described in Reed (1958), when a signal with a magnitude of A is fed from P1 in Fig. 2, the analytic expressions of the output amplitudes are

$$\begin{cases} A_1 = \dfrac{1}{2}\Gamma_{\mathrm{e}} + \dfrac{1}{2}\Gamma_{\mathrm{o}},\ A_2 = \dfrac{1}{2}T_{\mathrm{e}} + \dfrac{1}{2}T_{\mathrm{o}}, \\ A_3 = \dfrac{1}{2}T_{\mathrm{e}} - \dfrac{1}{2}T_{\mathrm{o}},\ A_4 = \dfrac{1}{2}\Gamma_{\mathrm{e}} - \dfrac{1}{2}\Gamma_{\mathrm{o}}. \end{cases} \tag{3}$$

Then, the scattering parameters can be written as

$$\begin{cases} S_{11} = \dfrac{1}{2}\Gamma_{\mathrm{e}} + \dfrac{1}{2}\Gamma_{\mathrm{o}},\ S_{21} = \dfrac{1}{2}T_{\mathrm{e}} + \dfrac{1}{2}T_{\mathrm{o}}, \\ S_{31} = \dfrac{1}{2}T_{\mathrm{e}} - \dfrac{1}{2}T_{\mathrm{o}},\ S_{41} = \dfrac{1}{2}\Gamma_{\mathrm{e}} - \dfrac{1}{2}\Gamma_{\mathrm{o}}. \end{cases} \tag{4}$$

To better compare other traditional structure hybrid couplers in a similar operation frequency, the center frequency of the improved hybrid coupler is set to 195 GHz. Then, according to Eqs. (1)–(4) and after some calculations, the initial dimensions are obtained as shown in Table 1. However, considering that the right angle cannot be machined during processing, a modified structure is designed to simplify the fabrication (Fig. 3). The radius of these circular cutouts is

Table 1 Parameters for the improved waveguide hybrid coupler with a center operating frequency of 195 GHz

Parameter	Length (mm)	Parameter	Length (mm)
T_1	0.38	W_1	0.30
T_2	0.14	W_2	0.16
L_1	0.54	W_3	0.14
L_2	0.67	W_4	0.40

0.3 mm, which can be easily fabricated using micromachining.

In addition, to demonstrate the feasibility of the modified structure, a comparison between simulations with and without modification is shown in Fig. 4. The simulation results show that the performance of the hybrid with modification is slightly poorer than that without modification, but the deterioration is still acceptable.

The computer model of the modified waveguide hybrid coupler is shown in Fig. 5. Specifically, an electromagnetic field distribution simulation is shown in Fig. 6, which demonstrates good power split performance and isolation characteristics of the design at 195 GHz. Furthermore, this new hybrid coupler geometry can achieve a wider operation bandwidth if more modified branches are used (Zhang et al., 2020).

In addition, the hybrid branch width should be large enough to use standard tools that typically have a width to depth aspect ratio (using standard E-plane split block fabrication) of less than 1/3 (Sobis et al., 2008). Compared to Rashid et al. (2014), the aspect ratio is 1:5.34, which is unbearable for the stress produced by the machine, and the modified branch structure has an aspect ratio of 1:1.82 in the standard waveguide WR-4.3. Furthermore, to make the comparison more reasonable, some hybrids working at the same operating frequency are selected. These hybrids have better tolerance performance than those presented in Sobis et al. (2008) and Rashid et al. (2014, 2016). According to the simulation results, when the parameters vary by 10 μm, the amplitude and phase imbalance will have a maximum change of only 0.1 dB and 0.5°, respectively.

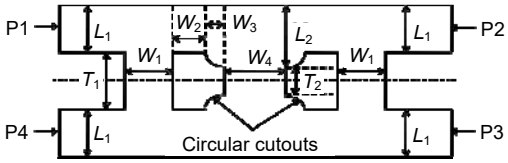

Fig. 3 Final structure of the improved three-branch hybrid coupler

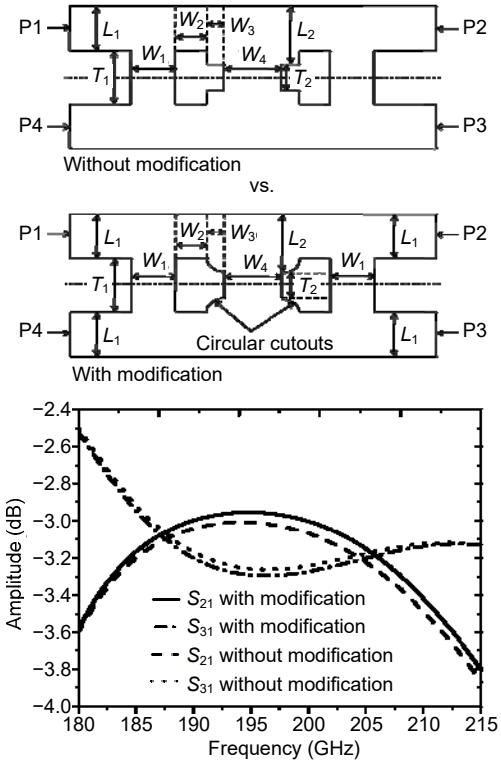

Fig. 4 Comparison between S_{21} and S_{31} parameters with and without modification

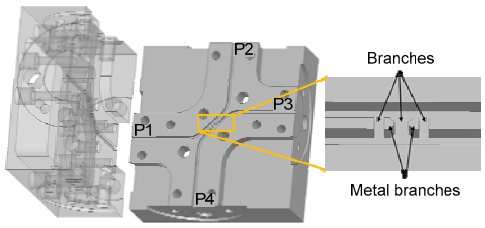

Fig. 5 Computer model of the designed E-plane 3-dB waveguide hybrid (the picture on the right shows the details of the circuit)

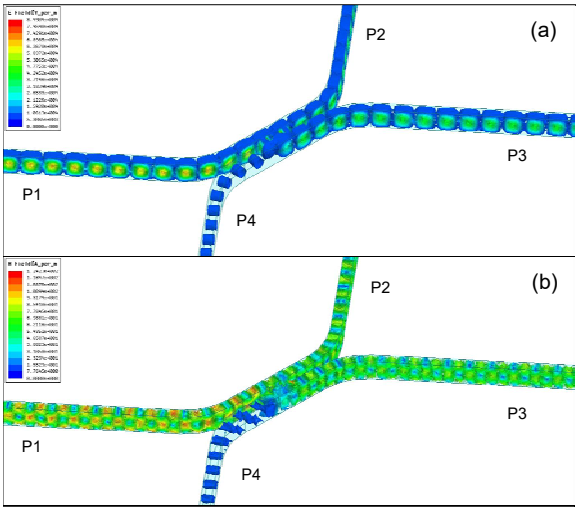

Fig. 6 Electromagnetic field distribution in the hybrid at 195 GHz: (a) electric field distribution; (b) magnetic field distribution

References to color refer to the online version of this figure

3 Simulation analysis of mechanical properties

When used for aerospace applications, the huge acceleration and shock could cause circuit deformation, which will influence or even damage the circuit. For waveguide hybrid couplers, the deformation of the branch will influence the hybrid ratio and phase imbalance. Therefore, some analysis of mechanical properties is required.

For mechanical reliability analysis of circuits such as waveguide hybrid couplers that have E-plane structural symmetry, to reduce the operation time, we can analyze only half of the circuit structure (one end fixed at the metal). This simplification does not affect the analysis of the overall stress trend of the whole device. Moreover, assuming that there are no machining defects, such as holes, cracks, and impurities in the packaging device, the temperature is continuous at the interface, and the interface is in good contact. If there is a defect in the assembly process, the shock resistance of the device may be greatly reduced. This is beyond the scope of this article.

For comparison, three models are built and simulated together. A indicates the metal block, B is the modified metal branch structure, C is with the same size as B without circular cutouts at the top and bottom, and D is the narrowest metal branch structure in Sobis et al. (2008) (because the operation frequency of the hybrid coupler is almost the same as that of the presented modified coupler). The mechanical analysis model is based on the provided High-Frequency Structure Simulator (HFSS) three-dimensional (3D) models, and then remodeling and local simplification are done through ANSYS Workbench software. Besides, the parts are under complicated forces and the whole model is manually dispersed to obtain a more reasonable and reliable result; the final grid discrete model in ANSYS Workbench is shown in Fig. 7.

For a comprehensive analysis and to obtain reasonable results, stress simulation has been analyzed from three directions, the direction perpendicular to the metal branch models (X and Y axes) and the direction parallel to the metal branch models (Z axis), as shown in Fig. 8. Then, it is found that for all models, when the stress is the same or under the same acceleration, the deformation of the metal branch varies

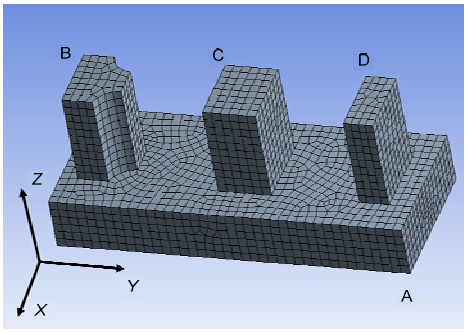

Fig. 7 Grid discrete model for three metal branch structures

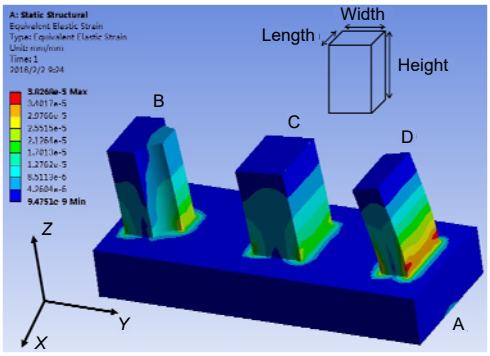

Fig. 8 Stress nephogram of the three branches, where structure D has the maximum structural deformation and displacement

References to color refer to the online version of this figure

most along the Y axis. Therefore, the analysis of deformation under stress that extends toward the Y axis is focused.

Different from a ground and aeronautical device, a space-borne device concerns mainly the effect of impact on the product during ground transportation and the launching process. These processes are relatively short to generate fatigue failures. Therefore, the main consideration is the random vibration and equivalent stress produced during the impact process.

Then, according to the generalized Hooke law, when the stress is less than the yield limit, the deformation of the branch is directly proportional to the stress, i.e., $\sigma=E\varepsilon$, where σ is the stress, ε is the strain, and E is Young's modulus. Fig. 9 shows that the displacements of the top of the branch for these three structures vary with different accelerations when the block material is aluminum or copper (materials usually used for circuit blocks). In the figure, the solid point means that the stress reaches the material's yield

limit and will soon fracture. The three structures are under the same acceleration. The block material is aluminum in Fig. 9a. The results show that the displacement of B is almost the same as that of C, but it is 22% smaller than that of D. Besides, when the acceleration increases to 40*g* (*g* is the acceleration of gravity), structure D reaches its limit for deformation and fractures, whereas structure B fractures when the acceleration is more than 50*g*. As for copper, the trend of displacement variation is identical, but D fractures when the acceleration is 26.5*g* and B fractures at 34.1*g* (Fig. 9b).

For a more comprehensive research and analysis of hybrids working in other frequencies, the displacement of the branch varying with the width-length ratio and height-length ratio has also been studied. Fig. 10 shows the displacement of the general rectangle branch changing with varying width-length ratio and height-length ratio at a particular acceleration. To determine the change rules between these parameters, the yield limit is not considered in this graph. When the width-length ratio decreases and the height-length ratio increases, the metal branch displacement becomes larger.

4 Measurement and results

From a space application perspective, cost is important in addition to mechanical reliability. For instance, when the narrowest branch width is 0.3 mm, the manufacturing cost is only half of that of the 0.15-mm narrowest branch width and a quarter of that of the 0.07-mm narrowest branch width.

Therefore, the narrowest branch of the modified waveguide hybrid is optimized to 0.3 mm. The block is manufactured in a micromachining system with a 0.3-mm diameter and a 1-mm long cutter tool and machined out of an aluminum block. A photograph of the block is shown in Fig. 11. There are four platforms on the corners of the hybrid block that are used to avoid separating screw holes and to ensure that

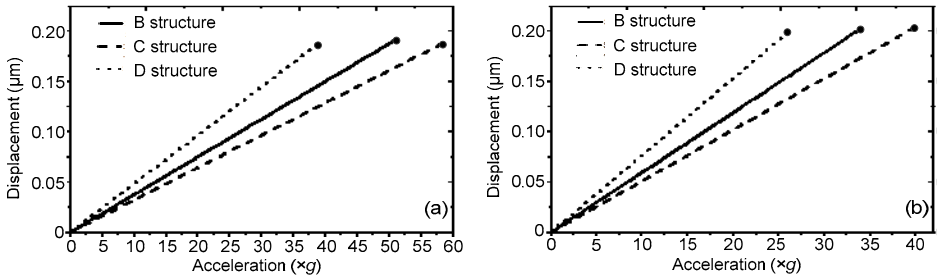

Fig. 9 Displacement of the top of the branch varying with acceleration regarding these three structures: (a) aluminum; (b) copper

The solid point means that the stress reaches the material's yield limit and will soon fracture

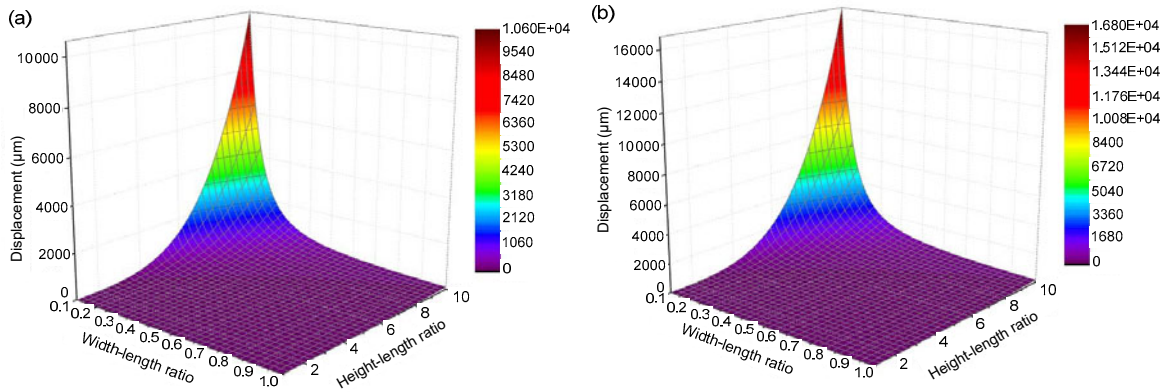

Fig. 10 Displacement of the general rectangle branches changing with varying width-length ratio and height-length ratio (the length value is 0.39 mm) at a certain acceleration of the random vibration at 20.3*g* when the block material is aluminum (a) or copper (b)

References to color refer to the online version of this figure

waveguides and branches are perfectly aligned when the blocks are combined. To make the experiment more reasonable, a 200-GHz traditional structure branch hybrid with the same and narrowest metal branch as the D structure in the mechanical property simulation part is also fabricated.

The simulation results need to be proven through experimentation. The random vibration experiment platform is based on the LDS test and Measurement's V8-440 metric shaker system (Fig. 12). According to the space-level reliability qualification, the experimental condition of the random vibration is 10–200 Hz: +6 dB / Otc, 200–1500 Hz: $0.25g^2$ / Hz, and 1500–2000 Hz: −12 dB / Otc. The total root mean square acceleration is 20.3*g* and the experimental time is 1 h along the *Y* axis.

In addition, the impact experimental platform is based on Dongling Tech's ES-200LS3-650 electrodynamic vibration system (Fig. 13). The experimental condition is 100–400 Hz: +6 dB / Otc and 400–4000 Hz: 400*g* along the *Y* axis.

The waveguide hybrid is measured before and after the vibration experiment using a Ceyear AV3672C two-port vector network analyzer (VNA) with AV3649 170–220 GHz extension transmitter and receiver modules. The measurement setup is shown in Fig. 14. The VNA testing system uses the TRL (thru-reflect-line) method for calibration. After calibration, it is important to restrict the movement of the cable that connects the VNA and the frequency converter to

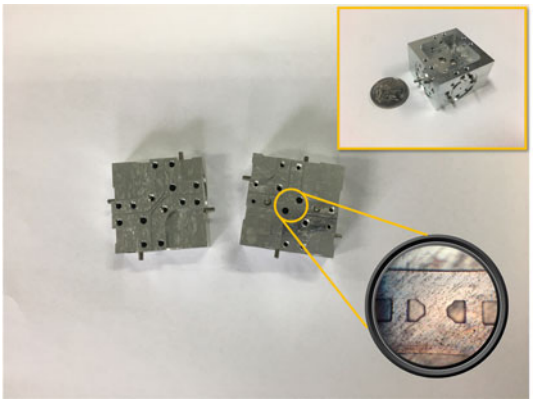

Fig. 11 Photograph of the two pieces of E-plane waveguide split-block
The inset photo shows the whole block of the hybrid, whereas the photo at the bottom right corner shows the hybrid circuit under the microscope

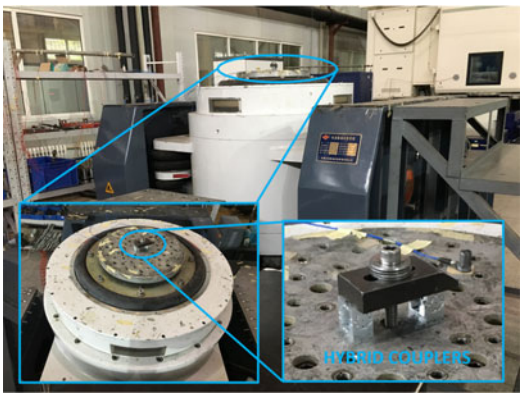

Fig. 13 Photographs of the impact experimental platform
The traditional structure hybrid coupler and the modified structure hybrid coupler are fixed in the impact platform

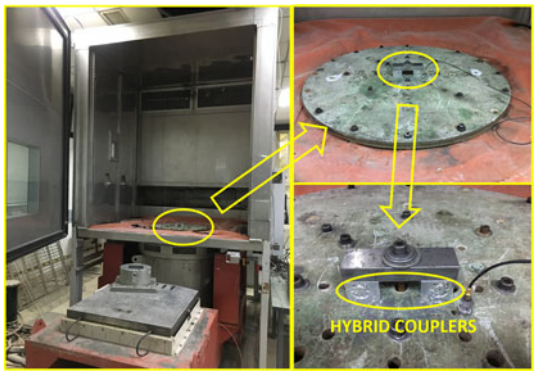

Fig. 12 Photographs of the random vibration experimental platform including the V8-440 shaker and the thermostat
The traditional structure hybrid coupler and the modified structure hybrid coupler are fixed in the vibration platform

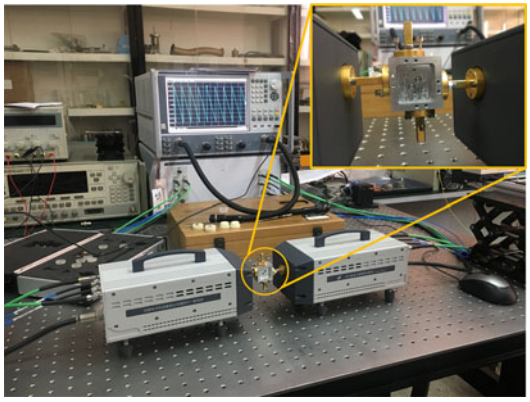

Fig. 14 Photograph of the measurement setup, including the 170–220 GHz extension modules with the connected waveguide hybrid
The inset photo shows that the remaining ports are terminated with matched loads during measurements

avoid making the calibration data worse, especially when measuring the phase of the ports. Because the hybrid is a four-port device but the VNA is a two-port testing system, when two ports are under measurement, the remaining ports need to be terminated with waveguide-matched loads from the calibration kit.

S-parameter measurement results of the hybrid are presented in Figs. 15–17. For the modified hybrid coupler, the comparison of the amplitude imbalance measurement results before and after the vibration experiment is shown in Fig. 15a. Fig. 15b shows the amplitude imbalance measurement results of the

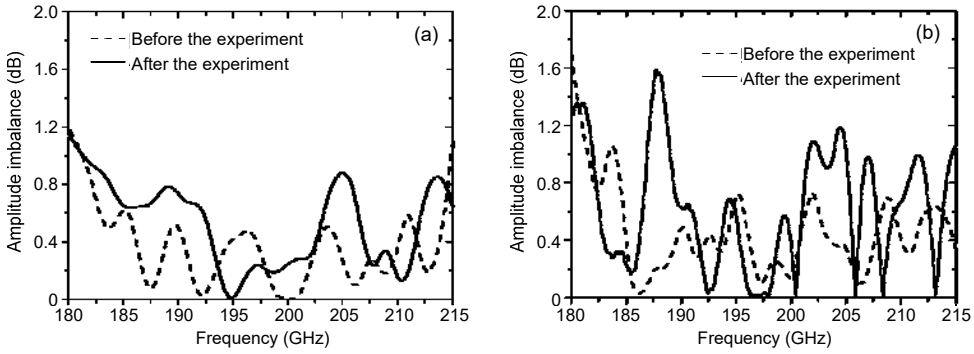

Fig. 15 Measured and simulated amplitude imbalances of the modified branch hybrid coupler (a) and the traditional structure hybrid coupler (b)

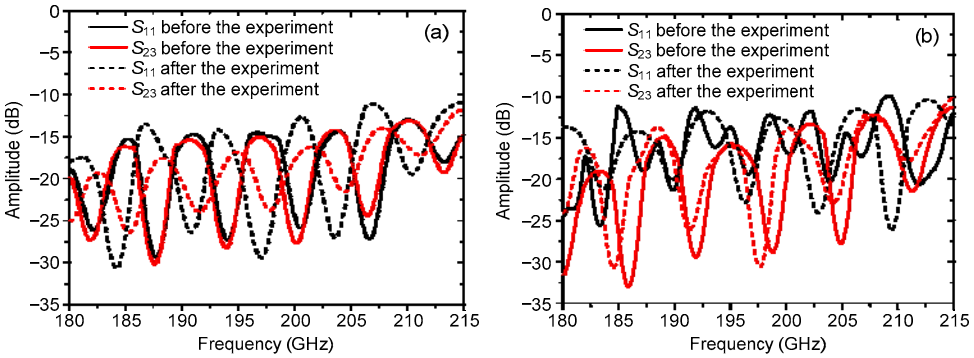

Fig. 16 Measured and simulated reflection loss (S_{11}) and isolation (S_{23}) of the modified branch hybrid coupler (a) and the traditional structure hybrid coupler (b)

References to color refer to the online version of this figure

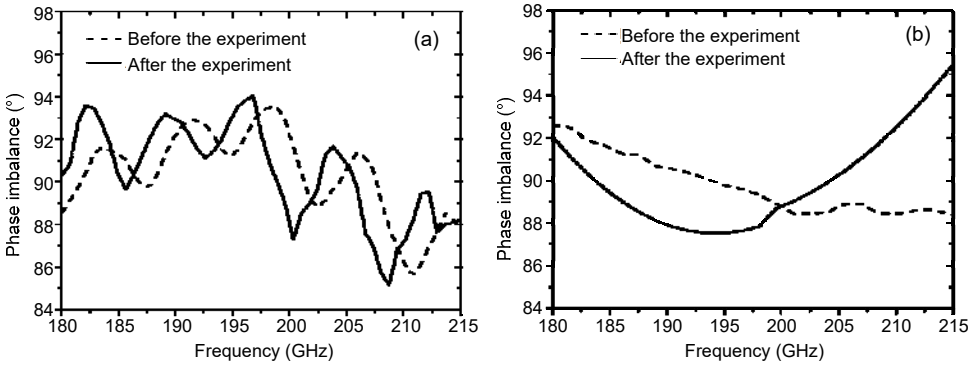

Fig. 17 Measured and simulated phase imbalances of the modified branch hybrid coupler (a) and the traditional structure hybrid coupler (b)

traditional structure hybrid coupler. In addition, for the modified hybrid coupler, the comparison of S_{11} and S_{23} measurement results before and after the vibration experiment is shown in Fig. 16a. Fig. 16b shows S_{11} and S_{23} measurement results of the traditional hybrid coupler. The results show that the vibration experiment can deteriorate the coupling performance of the hybrid coupler, and that the performance of the traditional hybrid coupler becomes worse than that of the modified hybrid coupler after the experiment. For the modified hybrid coupler, the comparison of the phase imbalance measurement results before and after the vibration experiment is shown in Fig. 17a. Fig. 17b shows the phase imbalance measurement results of the traditional structure hybrid coupler, showing agreement with the simulation results.

5 Conclusions

In this paper, a comprehensive mechanical reliability study of 3-dB waveguide hybrid couplers in submillimeter and terahertz bands has been presented. By concentrating on the analysis of the displacement variation with different width-length ratios and height-length ratios caused by random impact vibrations in the couplers, the necessity of improving the mechanical properties of the coupler's branch has been shown.

A mechanical study of 3-dB hybrid couplers has been experimentally verified by setting up a vibration experiment for the novel branch coupler and the traditional five-branch hybrid coupler. The measurement results showed that the vibration experiment can deteriorate the coupling performance of the hybrid coupler. An additional benefit from the structure is that the modified structure hybrid coupler has great tolerance performance. After the vibration experiment, the performance of the coupler was better than that of the traditional structure hybrid coupler. More importantly, the experiment conducted is just one impact experiment and only a one-hour vibration experiment. However, during the real applications, the circuit will be faced with dozens of impact occurrences and hours of vibration, and the deterioration of hybrid circuit can be even worse.

In summary, when used for an aerospace application, the displacement of the branch caused by random vibration or impact stress cannot be ignored. Therefore, mechanical properties of the hybrid branch need to be considered.

Contributors

Zhongqian NIU and Bo ZHANG designed the research. Zhongqian NIU processed the data. Dongfeng JI, Yang LIU, Yinian FENG, and Tianchi ZHOU helped conduct the experiment. Zhongqian NIU drafted the manuscript. Daotong LI and Yaohui ZHANG helped organize the manuscript. Bo ZHANG, Daotong LI, and Yong FAN revised and finalized the paper.

Acknowledgements

The authors would like to thank Mr. H. YING for the help in the vibration measurement. The authors would also like to thank Mr. L. C. NIU from China Railway Rolling Stock Corporation (CRRC) for the fruitful mechanical property discussions.

Compliance with ethics guidelines

Zhongqian NIU, Bo ZHANG, Daotong LI, Dongfeng JI, Yang LIU, Yinian FENG, Tianchi ZHOU, Yaohui ZHANG, and Yong FAN declare that they have no conflict of interest.

References

Armstrong CM, 2012. The truth about terahertz. *IEEE Spectr*, 49(9):36-41. https://doi.org/10.1109/MSPEC.2012.6281131

Chattopadhyay G, 2011. Technology, capabilities, and performance of low power terahertz sources. *IEEE Trans Terahertz Sci Technol*, 1(1):33-53. https://doi.org/10.1109/TTHZ.2011.2159561

Chen Z, Zhang B, Zhang Y, et al., 2016a. 220 GHz outdoor wireless communication system based on a Schottky-diode transceiver. *IEICE Electron Expr*, 13(9):1-9. https://doi.org/10.1587/elex.13.20160282

Chen Z, Wang H, Alderman B, et al., 2016b. 190 GHz high power input frequency doubler based on Schottky diodes and AlN substrate. *IEICE Electron Expr*, 13(22):1-12. https://doi.org/10.1587/elex.13.20160981

Dhillon SS, Vitiello MS, Linfield EH, et al., 2017. The 2017 terahertz science and technology roadmap. *J Phys D Appl Phys*, 50(4):043001. https://doi.org/10.1088/1361-6463/50/4/043001

Gonzalez A, Kojima T, Kaneko K, et al., 2017. 275–500 GHz waveguide diplexer to combine local oscillators for different frequency bands. *IEEE Trans Terahertz Sci Technol*, 7(6):669-676. https://doi.org/10.1109/TTHZ.2017.2758789

Graham-Rowe D, 2007. Terahertz takes to the stage. *Nat Photon*, 1(2):75-77. https://doi.org/10.1038/nphoton.2006.85

Hesper R, Khudchenko A, Baryshev AM, et al., 2017. A high-

performance 650-GHz sideband-separating mixer—design and results. *IEEE Trans Terahertz Sci Technol*, 7(6):686-693. https://doi.org/10.1109/TTHZ.2017.2758270

Hosako I, Sekine N, Patrashin M, et al., 2007. At the dawn of a new era in terahertz technology. *Proc IEEE*, 95(8):1611-1623. https://doi.org/10.1109/JPROC.2007.898844

Kooi JW, Chamberlin RA, Monje R, et al., 2012. Balanced receiver technology development for the Caltech Submillimeter Observatory. *IEEE Trans Terahertz Sci Technol*, 2(1):71-82. https://doi.org/10.1109/TTHZ.2011.2177726

Lubecke VM, Mizuno K, Rebeiz GM, 1998. Micromachining for terahertz applications. *IEEE Trans Microw Theory Techn*, 46(11):1821-1831. https://doi.org/10.1109/22.734493

Malo-Gomez I, Gallego-Puyol JD, Diez-Gonzalez C, et al., 2009. Cryogenic hybrid coupler for ultra-low-noise radio astronomy balanced amplifiers. *IEEE Trans Microw Theory Techn*, 57(12):3239-3245. https://doi.org/10.1109/TMTT.2009.2033874

Müller J, Pham MN, Jacob AF, 2011. Directional coupler compensation with optimally positioned capacitances. *IEEE Trans Microw Theory Techn*, 59(11):2824-2832. https://doi.org/10.1109/TMTT.2011.2165961

Niu ZQ, Zhang B, Yang K, et al., 2019a. Mode analyzing method for fast design of branch waveguide coupler. *IEEE Trans Microw Theory Techn*, 67(12):4733-4740. https://doi.org/10.1109/TMTT.2019.2944598

Niu ZQ, Zhang B, Ji DF, et al., 2019b. A novel 3-dB waveguide hybrid coupler for terahertz operation. *IEEE Microw Wirel Compon Lett*, 4(29):273-275. https://doi.org/10.1109/LMWC.2019.2899760

Phromloungsri R, Chongcheawchamnan M, Robertson ID, 2006. Inductively compensated parallel coupled microstrip lines and their applications. *IEEE Trans Microw Theory Techn*, 54(9):3571-3582. https://doi.org/10.1109/TMTT.2006.881026

Rashid H, Meledin D, Desmaris V, et al., 2014. Novel waveguide 3 dB hybrid with improved amplitude imbalance. *IEEE Microw Compon Lett*, 24(4):212-214. https://doi.org/10.1109/LMWC.2013.2293671

Rashid H, Desmaris V, Belitsky V, et al., 2016. Design of wideband waveguide hybrid with ultra-low amplitude imbalance. *IEEE Trans Terahertz Sci Technol*, 6(1):83-90. https://doi.org/10.1109/TTHZ.2015.2502070

Reed J, 1958. The multiple branch waveguide coupler. *IRE Trans Microw Theory Techn*, 6(4):398-403. https://doi.org/10.1109/TMTT.1958.1125213

Siles JV, Maestrini A, Alderman B, et al., 2011. A single-waveguide in-phase power-combined frequency doubler at 190 GHz. *IEEE Microw Wirel Compon Lett*, 21(6):332-334. https://doi.org/10.1109/LMWC.2011.2134080

Sobis PJ, Stake J, Emrich A, 2008. A 170 GHz 45° hybrid for submillimeter wave sideband separating subharmonic mixers. *IEEE Microw Wirel Compon Lett*, 18(10):680-682. https://doi.org/10.1109/LMWC.2008.2003463

Tonouchi M, 2007. Cutting-edge terahertz technology. *Nat Photon*, 1(2):97-105. https://doi.org/10.1038/nphoton.2007.3

Zhang B, Niu ZQ, Wang JL, et al., 2020. Four-hundred gigahertz broadband multi-branch waveguide coupler. *IET Microw Antenn Propag*, 14(11):1175-1179. https://doi.org/10.1049/iet-map.2020.0090

Zhou YF, Hu J, Liu S, et al., 2014. A terahertz-band branch waveguide directional coupler based on micro-machining. Int Conf on Communication Problem-Solving, p.223-226. https://doi.org/10.1109/ICCPS.2014.7062258